
White Rose Research Online

eprints@whiterose.ac.uk
https://eprints.whiterose.ac.uk
Universities of Leeds, Sheffield and York

Deposited via The University of York.

White Rose Research Online URL for this paper:
https://eprints.whiterose.ac.uk/id/eprint/246174/

Preprint:
Chen, S., Petri, M., Paschalis, S. et al. (2026) Electromagnetic transition strength in ^{53}Ca: the lifetime of the $5/2^{-}$ state. [Preprint]

Reuse
Items deposited in White Rose Research Online are protected by copyright, with all rights reserved unless indicated otherwise. They may be downloaded and/or printed for private study, or other acts as permitted by national copyright laws. The publisher or other rights holders may allow further reproduction and re-use of the full text version. This is indicated by the licence information on the White Rose Research Online record for the item.

Takedown
If you consider content in White Rose Research Online to be in breach of UK law, please notify us by emailing eprints@whiterose.ac.uk including the URL of the record and the reason for the withdrawal request.





Electromagnetic transition strength in ^{53}Ca: the lifetime of the $5/2^-$ state

S. Chen[a], M. Petri[a], S. Paschalis[a], H. L. Crawford[b], P. Doornenbal[c], R. Taniuchi[a], K. Wimmer[d,e,c], B. A. Brown[f], J. D. Holt[g,h], B. S. Hu[i], T. Miyagi[j], T. Otsuka[c,e,k], Y. Tsunoda[j], N. Aoi[l], H. Baba[c], M. Bentley[a], F. Browne[c], C. Campbell[b], Z. Chen[m], R. Crane[a], H. de Witte[n], P. Fallon[b], C. Fransen[o], H. Hess[o], E. Ideguchi[l], S. Iwazaki[l], J. Kim[p], A. Kohda[l], T. Koiwai[e], W. Marshall[a], B. Mauss[c], B. Moon[q,c], T. Parry[r], P. Reiter[o], H. Sakurai[c,e], D. Suzuki[e,s,c], L. Tetley[a], S. Thiel[o], Y. Yamamoto[l]

[a]*School of Physics, Engineering and Technology, University of York, Heslington, York YO10 5DD, UK*
[b]*Nuclear Science Division, Lawrence Berkeley National Laboratory, Berkeley, California 94720, USA*
[c]*RIKEN Nishina Center, 2-1 Hirosawa, Wako, Saitama 351-0198, Japan*
[d]*Instituto de Estructura de la Materia, CSIC, E-28006 Madrid, Spain*
[e]*Department of Physics, University of Tokyo, 7-3-1 Hongo, Bunkyo, Tokyo 113-0033, Japan*
[f]*Department of Physics and Astronomy and the Facility for Rare Isotope Beams, Michigan State University, East Lansing, MI 48824-1321, USA*
[g]*TRIUMF 4004 Wesbrook Mall, Vancouver, British Columbia V6T 2A3, Canada*
[h]*Department of Physics, McGill University, Montréal, QC H3A 2T8, Canada*
[i]*Cyclotron Institute and Department of Physics and Astronomy, Texas A&M University, College Station, Texas 77843, USA*
[j]*Center for Computational Sciences, University of Tsukuba, 1-1-1 Tennodai, Tsukuba 305-8577, Japan*
[k]*Advanced Science Research Center, Japan Atomic Energy Agency, Tokai, Japan*
[l]*Research Center for Nuclear Physics (RCNP), Osaka University, Mihogakoa, Ibaraki, Osaka 567-0047, Japan*
[m]*GSI Helmoltzzentrum für Schwerionenforschung GmbH, Planckstr. 1, 64291 Darmstadt, Germany*
[n]*Institute for Nuclear and Radiation Physics, KU Leuven, Leuven B-3001, Belgium*
[o]*Institut für Kernphysik, Universität zu Köln, D-50937 Cologne, Germany*
[p]*Department of Physics, Korea University, Seoul 02841, Republic of Korea*
[q]*Center for Exotic Nuclear Studies, Institute for Basic Science, Daejeon, 34126, Republic of Korea*
[r]*Department of Physics, University of Surrey, Guildford GU2 7XH, UK*
[s]*Quark Nuclear Science Institute, the University of Tokyo, 7-3-1 Hongo, Bunkyo, Tokyo 113-0033, Japan*

arXiv:2609.23754v1 [nucl-ex] 20 Sep 2026

Abstract

High-resolution in-beam γ-ray spectroscopy of ^{53}Ca was performed at the Radioactive Isotope Beam Factory (RIBF) at RIKEN. Excited states in ^{53}Ca were populated via one-neutron and one-proton removal reactions from a ^{55}Sc radioactive beam, and the emitted γ rays were detected using the HiCARI hybrid germanium detector array. The lifetime of the first excited $5/2^-$ state in ^{53}Ca was measured for the first time through an analysis of Doppler-broadened γ-ray line shapes arising from relativistic recoil velocities. A lifetime of $\tau = 11.3^{+5.3(\mathrm{stat})+3(\mathrm{sys})}_{-11.3}$ ps was deduced, corresponding to a reduced transition probability of $B(E2; 5/2^- \rightarrow 1/2^-) > 2.6\ e^2fm^4$ at the 1σ level, with a best-fit value of $4.5\ e^2fm^4$. The measured transition strength is compared with state-of-the-art shell-model and *ab initio* calculations, providing a stringent benchmark for shell-model Hamiltonians and effective charges and modern *ab initio* descriptions of the neutron-rich calcium isotopes approaching the potential $N = 40$ shell closure.

1. Introduction

Nuclear magic numbers provide the cornerstones of our understanding of nuclear structure. These numbers define the shell gaps and emergent phenomena of nuclear deformation, which appear in open-shell nuclei, giving rise to collective motion. However, their universality does not extend to exotic nuclei; some magic numbers vanish, while new ones appear away from the valley of stability. Nucleon-nucleon correlations are responsible for the modification of nuclear structure away from the valley of stability. Indeed, the isospin dependence of the monopole average of the central, tensor, and 2-body spin-orbit forces affects the effective single-particle energies and drives systems from magic, to deformed, and even to superfluid. Understanding and quantitatively describing properties of nuclei away from the valley of stability is at the forefront of nuclear structure science.

The calcium isotopic chain has provided great input into our understanding of shell evolution, with new sub-shell gaps appearing at $N = 32$ [1] and $N = 34$ [2]. Beyond ^{54}Ca, the next potential shell closure is at $N = 40$, marking the filling of the neutron $f_{5/2}$ orbital. The newly developed fp shell interaction, UFP-CA [3], fitted existing experimental data in calcium isotopes, including the excitation energies up to ^{54}Ca, and allows extrapolated predictions out to ^{60}Ca. It predicts that ^{60}Ca is doubly magic at a similar level to ^{68}Ni [3]. In contrast, the first spectroscopy measurements of ^{56,58}Ca were recently performed at RIBF [4]. The observed excitation energies, along with other experimental data on calcium isotopes, were used to refine the A3DA-m interaction in the $fpg_{9/2}d_{5/2}$ model space, which was named A3DA-t and predicted that ^{60}Ca is not doubly magic and that the dripline of calcium isotopes extends to at least $N = 50$ [4]. Additionally, low-lying states in ^{55,57}Ca [5] and ^{62}Ti [6] were observed in the same experiment, also suggesting that the $N = 40$ island of inversion extends down to calcium isotopes.

There are still many open questions regarding the magicity

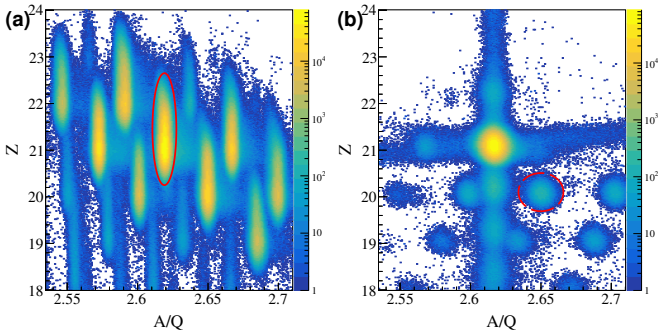


Figure 1: (a) Incoming beam particle identification in the BigRIPS separator. The solid ellipse indicates the ^{55}Sc. (b) Reaction residue particle identification in the ZeroDegree spectrometer for the ^{55}Sc incoming beam. The dashed ellipse indicates the ^{53}Ca.

of ^{60}Ca [3, 7, 4]. In view of the difficulties of currently performing direct spectroscopy of ^{60}Ca (with planned upgrades of facilities and detection systems targeting exactly this region), a critical next step is to benchmark theory against other observables which are sensitive to physics beyond what is relevant for excitation energies alone. In particular, $B(E2)$ strengths beyond $N = 28$ ($Z = 20$) have been intermittently studied experimentally, and new data are urgently needed to guide our understanding of the Ca isotopic chain. In this article we report on the first measurement of the lifetime of the first excited state ($5/2^-$) of ^{53}Ca, and its $B(E2; 5/2^- \rightarrow 1/2^-)$ value, employing the HiCARI array at the RIBF facility and we compare this measurement with both shell-model calculations with effective charges, and *ab initio* calculations to test their description of this isotopic chain.

2. Experimental setup

The experiment was carried out at the Radioactive Isotope Beam Factory (RIBF) operated by the RIKEN Nishina Center and the Center for Nuclear Study (CNS), University of Tokyo. Radioactive beams in the neutron-rich calcium region were produced via the fragmentation of a ^{70}Zn primary beam on a ^{9}Be target at an energy of 345 MeV/nucleon. The fragments were selected using the BigRIPS separator [8] and identified on an event-by-event basis through the TOF-Bρ-ΔE measurements using the standard beam-line detectors described in Ref. [9]. These measurements enabled unambiguous particle identification in terms of mass-to-charge ratio and atomic number, as shown in Fig. 1(a). A 1 g/cm^2-thick carbon target and a 1.2 g/cm^2-thick polyethylene (CH_2) target were placed at the F8 focal plane to induce the knockout reactions. The ^{53}Ca nuclei in excited states were populated through the one-proton and one-neutron removal reaction (-1p-1n) from ^{55}Sc projectiles. The reaction residues were analyzed using the ZeroDegree spectrometer, applying the same method as in BigRIPS. Figure 1(b) shows the particle identification in the ZeroDegree spectrometer gated on the incoming ^{55}Sc beam.

The prompt γ rays emitted following the knockout reactions were detected using the High-resolution Cluster Array at RIBF (HiCARI) [10]. HiCARI is a hybrid array composed of multiple types of segmented high-purity germanium detectors. In this experiment, six Miniball triple-cluster detectors (six-fold segmented) [11] were positioned at forward angles, covering 20° – 55° relative to the beam axis. Four clover detectors (four-fold segmented) [12] were mounted to cover 60° – 85°, and two GRETINA-type tracking detector clusters [13] were placed covering 50° – 90°. The detector configuration is shown in Fig. 2 of Ref. [14]. Each detector was calibrated individually using ^{133}Ba, ^{152}Eu, and ^{60}Co γ-ray sources. The Doppler correction was performed by taking the point of highest energy deposit as the initial photon interaction. For the Miniball and clover detectors, the position of highest energy deposit segment – pre-determined from simulations as the average first interaction point for each segment – was used to calculate the γ-ray emission angle. For the tracking detectors, pulse-shape analysis [15] was employed to determine the γ-ray interaction positions within the crystal volume with a precision of a few millimeters. Ultimately, the tracking detectors provided significantly superior energy resolution and peak-to-Compton ratios in the Doppler-corrected spectra compared with the Miniball and clover detectors, leading to higher sensitivity to the short lifetimes measured in this experiment. Therefore, only the tracking detectors were used in the subsequent analysis.

3. Results

For the γ-ray analysis, Doppler corrections were applied using the mid-target velocities, deduced event-by-event from the beam velocities measured with BigRIPS and ZeroDegree, accounting for the energy loss in the target material and beam-line detectors. The γ-ray emission point was assumed to be at the center of the target. To improve the peak-to-Compton ratio, add-back analysis was performed by summing the detected energies within each cluster.

The resulting Doppler-corrected γ-ray spectra for ^{36}Ar (populated in -1p from ^{37}K) and ^{53}Ca are shown in Fig. 2 and 3, respectively. The observed spectral lineshapes are governed by three main factors: the intrinsic detector energy resolution, the velocity spread of the emitting nucleus, and the uncertainty in the γ-ray emission angle. The lifetime affects both the velocity distribution at the time of γ-ray emission and the angular uncertainty, thereby modifying the lineshape. To extract lifetimes from the observed lineshapes, the experimental spectra were compared with simulated response functions generated under different lifetime assumptions. These simulations were performed using a customized Geant4 [16] simulation package derived from the GRETINA simulation software [17]. To reproduce the experimental lineshapes, the simulations incorporated the real target thickness and the measured beam profile, and energy resolutions obtained from source calibrations were implemented for each detector. The effective position resolution of the tracking detectors – critical for controlling the angular uncertainty – was determined from the benchmark channel described below. Doppler corrections were applied to the simulated data in the same manner as for the experimental data to ensure consistency.

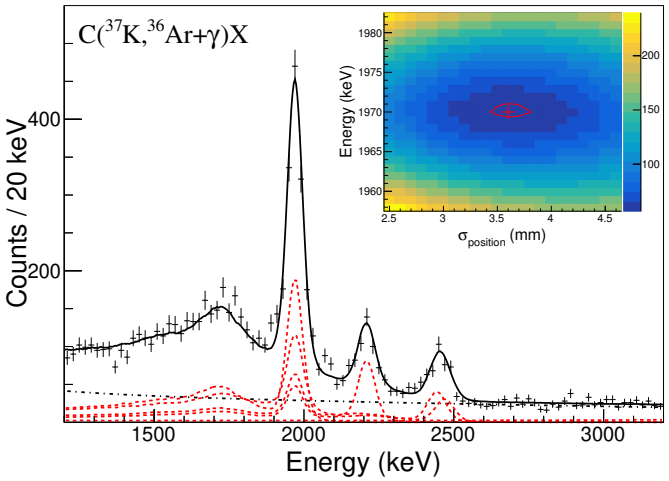


Figure 2: Doppler-corrected γ-ray energy spectrum of ^{36}Ar, populated via one-proton removal from ^{37}K on the carbon target, measured with the tracking detectors. The spectrum is fitted using simulated response functions with the final position resolution (red dashed line) on top of a double-exponential background (black dash-dotted line). The inset shows the χ^2 surface for the $2^+_1 \rightarrow 0^+_{g.s}$ transition obtained by varying the transition energy and γ-ray interaction position resolution in the simulation. The red cross marks the $\chi^2_{\rm min}$, and the red contour indicates the 1σ confidence region ($\chi^2_{\rm min}+1$).

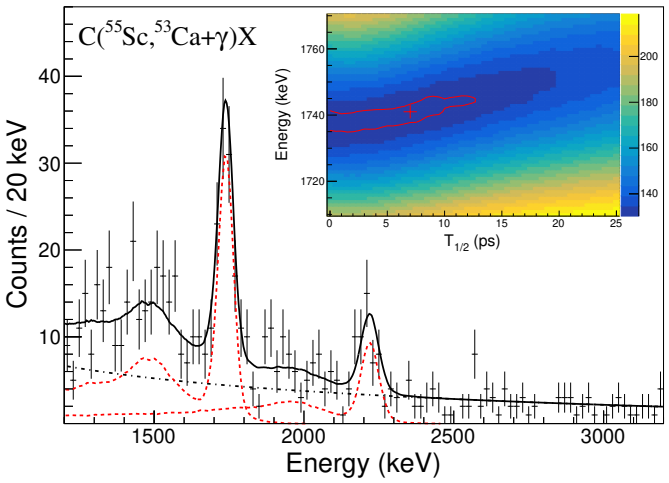


Figure 3: The same as Fig. 2 but for ^{53}Ca populated via one-proton and one-neutron removal from ^{55}Sc. The inset shows the χ^2 surface for the 1740-keV transition obtained by varying the transition energy and half-life in the simulation.

To benchmark the simulations, the spectra of ^{36}Ar were analyzed first. The low-lying excited states of ^{36}Ar are well established, with both excitation energies and lifetimes accurately determined in previous studies [18]. In this experiment, these excited states were populated via one-proton removal from a ^{37}K beam, produced using the same experimental setup but with BigRIPS and ZeroDegree tuned to the neutron-deficient side.

The Doppler-corrected ^{36}Ar spectrum obtained with the carbon target is shown in Fig. 2. Transitions from the 2^+_1, 4^+_1, 3^-_1, and 2^+_2 states are clearly observed. According to the literature [18], the 2^+_1 state (1970 keV, $T_{1/2}$ = 0.328 ps) decays directly to the ground state. The 4^+_1 (4414 keV, $T_{1/2}$ = 0.076 ps) and 3^-_1 (4178 keV, $T_{1/2}$ = 2.3 ps) states predominantly feed the 2^+_1 state, with negligible direct decay to the ground state. The 2^+_2 state (4440 keV, $T_{1/2}$ = 0.076 ps) decays to both the 2^+_1 and ground states with a branching ratio of 36:64. Simulations were therefore performed to generate response functions for cascade decay sequences of $2^+_1 \rightarrow 0^+_{\rm g.s.}$, $4^+_1 \rightarrow 2^+_1 \rightarrow 0^+_{\rm g.s.}$, $3^-_1 \rightarrow 2^+_1 \rightarrow 0^+_{\rm g.s.}$, $2^+_2 \rightarrow 2^+_1 \rightarrow 0^+_{\rm g.s.}$, and $2^+_2 \rightarrow 0^+_{\rm g.s.}$, using the literature transition energies and excited state lifetimes.

The simulated response functions were combined with a double-exponential background to fit the experimental spectrum. The amplitudes of the response functions and the background parameters were treated as free parameters in the fit. The branching ratio between the $2^+_2 \rightarrow 2^+_1 \rightarrow 0^+_{\rm g.s.}$ and $2^+_2 \rightarrow 0^+_{\rm g.s.}$ decay paths was fixed to the literature value.

To determine the position resolution of the tracking detectors, the lineshape of the most intense transition, $2^+_1 \rightarrow 0^+_{\rm g.s.}$ at 1970 keV, was investigated. In this study, the $2^+_1 \rightarrow 0^+_{\rm g.s.}$ transition energy – including those in the cascade decays – and the position resolution were varied simultaneously in the simulations, while all other transition energies and all $T_{1/2}$ values were fixed to their literature values. The resulting χ^2 surface as a function of the assumed transition energy and position resolution is shown in the inset of Fig. 2. The minimum, $\chi^2_{\rm min}$, was found at a transition energy of 1970 keV – consistent with the literature value – and a position resolution of σ = 3.6 mm. The extracted position resolution should be interpreted as an effective resolution that also accounts for uncertainties in the detector positions relative to the target. The fit using the simulated response functions with this final resolution is shown in Fig. 2, demonstrating good reproduction of the peak shapes and peak-to-Compton ratios observed in the experimental spectrum. An analogous analysis was carried out for the ^{36}Ar spectrum measured with the CH_2 target, resulting in an effective position resolution of σ = 3.8 mm.

The data analysis of ^{53}Ca followed the same procedure as that for ^{36}Ar. The Doppler-corrected ^{53}Ca spectrum measured with the carbon target is shown in Fig. 3. Excited states of ^{53}Ca were populated via one-proton and one-neutron removal from a ^{55}Sc beam, the same reaction used in Ref. [2]. The observed spectrum is consistent with that measured using the DALI2 NaI(Tl) array in Ref. [2], but with significantly improved energy resolution, enabling lifetime sensitivity.

Two transitions are observed and were interpreted as decays from the $5/2^-$ and $3/2^-$ states directly to the $1/2^-$ ground state [2]. These spin-parity assignments were supported by momentum-distribution analysis from knockout reactions in Ref. [19]. No additional bound excited states were observed in the high-statistic spectra reported in Refs. [2, 19]. As such, feeding from higher-lying state was not considered in the present lifetime analysis. Because of the limited statistics, the lifetime was extracted only for the stronger transition around 1.7 MeV. The transition around 2.2 MeV has previously been measured in β-decay spectroscopy with an energy of 2220(1) keV [20]. Accordingly, this transition was fixed to the literature energy and assumed to have a negligible lifetime in simulations. The transition around 1.7 MeV has been measured only in the in-beam γ-ray spectroscopy, with reported ener-

Table 1: Summary of transition energies E, lifetime τ, and reduced transition probabilities $B(E2)$ extracted for the $5/2^- \rightarrow 1/2^-$ transition in ^{53}Ca. Only statistical uncertainties are included.

	E (keV)	τ (ps)	$B(E2; 5/2^- \rightarrow 1/2^-)$ (e^2fm^4)
C target	1741^{+4}_{-6}	$10.1^{+7.9}_{-10.1}$	$5.1^{+\infty}_{-2.2}$
CH_2 target	1741^{+4}_{-7}	$12.3^{+7.2}_{-12.3}$	$4.2^{+\infty}_{-1.5}$
Weighted	1741^{+3}_{-5}	$11.3^{+5.3}_{-11.3}$	$4.5^{+\infty}_{-1.4}$

gies of 1753(15) keV in Ref. [2] and 1738(17) keV in Ref. [19]. Therefore, both the energy and lifetime of this transition were treated as free parameters and investigated simultaneously. The tracking detector position resolutions determined from the ^{36}Ar analysis were applied in the corresponding simulations for each target.

Similar to the ^{36}Ar case, the Doppler-corrected spectrum was fitted using simulated response functions combined with a double-exponential background. For each combination of transition energy and lifetime, the corresponding χ^2 value of the fit was evaluated. The inset of Fig. 3 shows the resulting χ^2 surface as a function of the assumed energy and half-life for the 1.7 MeV transition. The $\chi^2_{\rm min}$ is marked with a red cross, and the red contour indicates the 1σ confidence region ($\chi^2_{\rm min}$ + 1). The 1σ region extends down to zero in lifetime, reflecting the limited sensitivity of the present setup to short lifetimes. The fit using the simulated response functions with the best-fit energy and lifetime is shown in Fig. 3. An identical analysis of the ^{53}Ca spectrum measured with the CH_2 target yielded consistent results. The extracted transition energies and lifetimes are summarized in Table 1, where only statistical uncertainties are included. A weighted average of the results from both targets, using $1/\sigma^2$ as weights, gives final values of 1741^{+3}_{-5} keV and $\tau = 11.3^{+5.3}_{-11.3}$ ps. The deduced transition energy agrees with the values reported in Ref. [2, 19] within uncertainties.

Systematic uncertainties were also evaluated. The dominant contribution arises from the uncertainty in the position resolution. An uncertainty of 0.3 mm was adopted, based on the variation observed when extracting the position resolution for individual tracking clusters. When translated into lifetime uncertainty, a smaller assumed position resolution leads to a longer extracted lifetime, and vice versa. Since the statistical lower limit of the lifetime is already at zero, only the upper systematic limit needs to be considered. The same χ^2 studies were therefore repeated assuming a smaller position resolution. Under this assumption, the resulting 1σ region extends to a lifetime that is longer by 3 ps. A systematic uncertainty of +3 ps was thus adopted, yielding a final lifetime of $\tau = 11.3^{+5.3(\rm stat)+3(\rm sys)}_{-11.3}$ ps, and a reduced transition probability of $B(E2; 5/2^- \rightarrow 1/2^-) > 2.6\ e^2fm^4$ at the 1σ level, with a best-fit value of 4.5 e^2fm^4.

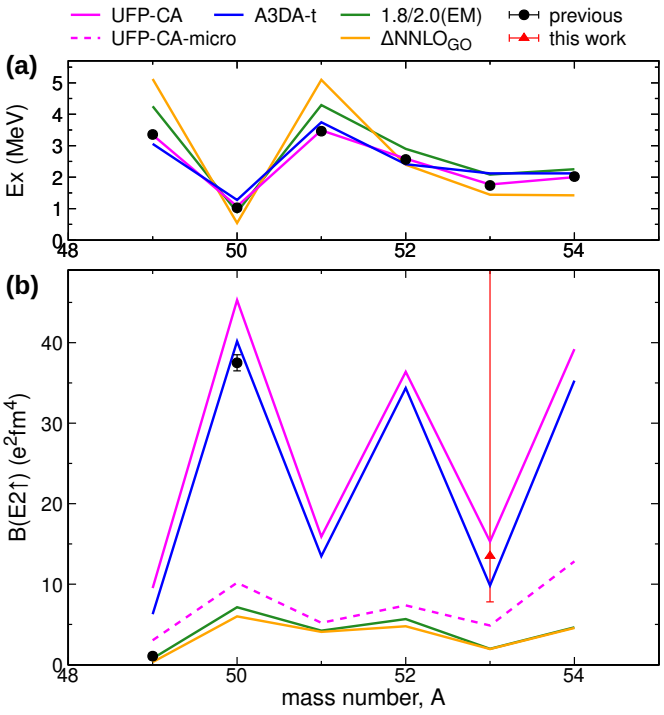


Figure 4: Systematic trend of excitation energies (a) and reduced transition probabilities (b) for the lowest $E2$ excitation in neutron-rich calcium isotopes as a function of mass number; $B(E2; 0^+ \rightarrow 2^+)$ for ^{50,52,54}Ca, $B(E2; 3/2^- \rightarrow 7/2^-)$ for ^{49,51}Ca and $B(E2; 1/2^- \rightarrow 5/2^-)$ for ^{53}Ca . The experimental results are compared with theoretical predictions from *ab initio* approaches and shell-model calculations. Experimental data are taken from Refs.[21, 22] and from the present work.

4. Discussion

In Fig. 4 we present the experimentally deduced reduced transition probabilities $B(E2\uparrow)$ for the lowest $E2$ excitations in neutron-rich calcium isotopes beyond the $N = 28$ shell, previously measured only for ^{49}Ca and ^{50}Ca and this work delivering the first measurement for ^{53}Ca. For ^{49}Ca, the value is taken from Ref. [21] for the $3/2^-_{\rm g.s.} \rightarrow 7/2^-$ excitation, while the value for ^{50}Ca is adopted from Ref. [22] for the $0^+_{\rm g.s.} \rightarrow 2^+$ excitation. Both literature values were deduced from lifetime measurements (using the Recoil Distance Doppler Shift method). The experimental results are compared with shell-model calculations employing the UFP-CA [3] and A3DA-t [4] interactions (with standard effective charges), as well as *ab initio* calculations using two NN+3N forces, 1.8/2.0(EM) [23, 24] and ΔNNLO$_{GO}$ [25], derived from chiral EFT. In addition, UFP-CA calculations with microscopically-treated effective charges (UFP-CA-micro) are shown. All calculations provide reasonable descriptions of the excitation energies (Fig. 4(a)). A more interesting picture emerges for the transition strengths shown in Fig. 4(b), which we will discuss separately for each theoretical approach (shell model vs *ab initio*).

4.1. Shell-model calculations and effective charges

For shell-model calculations, the $B(E2)$ depends on the effective-charge parameters e_p and e_n. The effective charges

Table 2: Reduced transition probabilities for the lowest $E2$ excitations in $^{47-53}$Ca isotopes. Experimental $B(E2)$ values are compared with shell-model calculations using KB3G, GXPF1Br, A3DA-t and UFP-CA Hamiltonians with standard $e_n = 0.5$ effective charge, and UFP-CA calculations with microscopically-treated effective charges.

	$E2$ transition	exp. $B(E2)$	$e_n = 0.5$ KB3G	$e_n = 0.5$ GXPF1Br	$e_n = 0.5$ A3DA-t	$e_n = 0.5$ UFP-CA	micro e_n UFP-CA	largest OBTD
^{47}Ca	$7/2^- \rightarrow 3/2^-$	2.0(1)	0.4	1.6	1.5	2.0	1.0	$p_{3/2} \rightarrow f_{7/2}$
^{48}Ca	$0^+ \rightarrow 2^+$	95(9)	57.7	51.8	52.8	67.5	27.5	$p_{3/2} \rightarrow f_{7/2}$
^{49}Ca	$3/2^- \rightarrow 7/2^-$	1.1(4)	0.8	7.1	6.1	9.5	3.0	$p_{3/2} \rightarrow f_{7/2}$
^{50}Ca	$0^+ \rightarrow 2^+$	37.5(1.1)	44.8	39.1	41.2	45.3	10.2	$p_{3/2} \rightarrow p_{3/2}$
^{51}Ca	$3/2^- \rightarrow 7/2^-$	–	13.8	13.4	13.7	15.9	5.2	$p_{3/2} \rightarrow f_{7/2}$
^{52}Ca	$0^+ \rightarrow 2^+$	–	38.1	30.8	36.7	36.4	7.4	$p_{1/2} \rightarrow p_{3/2}$
^{53}Ca	$1/2^- \rightarrow 5/2^-$	> 7.8	13.4	11.0	9.0	15.3	4.9	$p_{1/2} \rightarrow f_{5/2}$

account for the renormalization of the proton and neutron components of the $E2$ matrix elements within the shell-model basis of a major shell due to admixtures of the 1p-1h, $\Delta N = 2$ proton excitations. Effective charges are not expected to be constant as a function of increasing asymmetry (N, Z), but to have an approximate $1/A$ dependence, as understood by the macroscopic model of Bohr and Mottelson [26] and exemplified in [27], and by the microscopic calculations of Sagawa *et al.* [28] and Longfellow *et al.* [29].

Experimental $B(E2)$ values for the neutron-rich calcium isotopes are compared to calculations in Table 2. The theory includes those from two standard Hamiltonians for the pf model space, KB3G [30] and GXPF1Br [31, 2], together with the more recent A3DA-t [4] and UFP-CA [3] Hamiltonians. The $B(E2)$ are obtained with the standard value of $e_n = 0.5$ for the neutron effective charge from [31]. We use harmonic radial wavefunctions with $\hbar\omega = 45A^{-1/3} - 25A^{-2/3}$. For all of these Hamiltonians the one-body transition densities (OBTD) are dominated by one term given in the last column of Table 2. The calculated results for ^{50,51,52,53}Ca are similar for all three Hamiltonians and are in good agreement with experiment. The agreement for ^{50}Ca is improved if the slightly smaller effective charge from [32] of $e_n = 0.45$ is used.

For ^{42,44}Ca, the $B(E2)$ obtained in the pf model space are an order of magnitude smaller than experiment (see Fig. 17 in [29]). One must include sd to pf excitations for the low-lying intruder state and their mixing with the pf configurations [33]. The intruder states move up in energy as the neutron number increases, so that the wavefunctions above ^{46}Ca have more pure pf configurations. The factor of two larger experimental $B(E2)$ value for ^{48}Ca compared the pf calculations may be due to sd to pf admixtures.

For ^{47,49}Ca the calculated $B(E2)$ are relatively small and depend more strongly on the Hamiltonian. In the pf model space the wavefunctions are dominated by the simple configurations of

$$[(0f_{7/2})^7]\ (7/2^-) \rightarrow [(0f_{7/2})^6, J_f] \otimes [(1p_{3/2})]\ (3/2^-) \quad (1)$$

for ^{47}Ca and

$$[(0f_{7/2})^8] \otimes [1p_{3/2}]\ (3/2^-) \rightarrow [(0f_{7/2})^7, 7/2^-] \otimes [(1p_{3/2})^2, J_p]\ (7/2^-) \quad (2)$$

for ^{49}Ca. The largest calculated $B(E2)$ values come from the configurations with $J_f = J_p = 0$. However, the $B(E2)$ become reduced if there is admixture and interference with the components with $J_f = 2$ for ^{47}Ca and $J_p = 2$ for ^{49}Ca. In this regard, the mixing obtained with the KB3G Hamiltonian for ^{49}Ca is the only one that gives agreement with experiment.

The pf shell description for ^{47}Ca is analogous to the the sd description of the $5/2^+$ to $1/2^+$ transition discussed in [34] with dominant configurations

$$[(0d_{5/2})^5]\ (5/2^+) \rightarrow [(0d_{5/2})^4, J_d = 0] \otimes [(1s_{1/2})]\ (1/2^+) \quad (3)$$

Note that we can only have $J_d = 0$ for ^{21}O. In [34] it was noted that the sd calculation with the USDB Hamiltonian [35] and with the sd model space effective charge of $e_n = 0.45$ [36] gave a $B(E2)$ that was about a factor of two larger than experiment for this $5/2^+$ to $1/2^+$ transition in ^{21}O. This motivated discussion about the microscopic origin of the effective charge. We used the first-order model of [37] where the effective charge is obtained from an integral involving the valence transition density times the collective transition density for the giant quadrupole excitation that peaks near the nuclear surface. It was noted in this model that the effective charge for the $0d_{5/2}$ to $1s_{1/2}$ transition was reduced due to the crossing node in the $0d-1s$ valence transition density shown in Fig. 5. For ^{50}Ca and ^{52}Ca, the integral involving the p to p valence transition has a minimum at 3 fm as shown in Fig. 5. For the other cases in Table 2 involving p to f, the valence transition density crosses zero near 3 fm. This results in a small effective charge (see Table 3 in [29]). The $B(E2)$ obtained with the microscopic model are given in Table 2. The resulting $B(E2)$ for ^{50,53}Ca are about a factor of four smaller than experiment. This additional information indicates that the first-order model is inadequate. This leaves open the question as to why the experimental $B(E2)$ for ^{21}O is a factor of two smaller than the calculation.

4.2. *Ab initio calculations*

Ab initio theory has seen rapid recent progress for descriptions of ground-state energies and radii as well as the excitation spectrum. First microscopic calculations [38, 39, 40] have also highlighted the calcium isotopes as a key isotopic chain to test

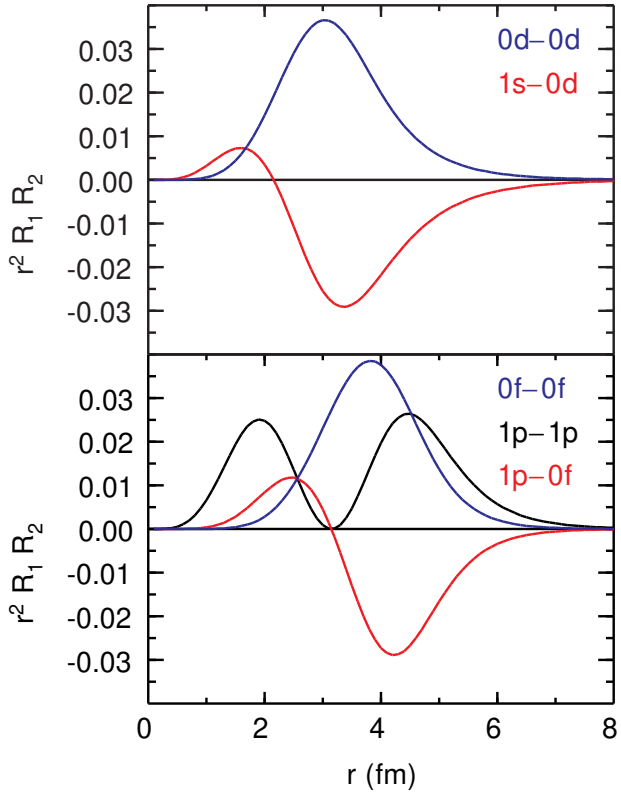


Figure 5: Radial parts of the valence single-particle $E2$ transition densities for the neutrons in the *sd* shell for ^{22}O (top), and for neutrons in the *pf* shell for ^{48}Ca (bottom).

the role of 3N forces in the quest for a microscopic description of the atomic nucleus using realistic interactions originating from chiral EFTs. *Ab initio* calculations of masses, charge radii, and low-lying spectroscopy have also been performed for neutron-rich calcium isotopes [41, 42, 43, 4, 5, 6]. The critical next step is the description of electromagnetic observables, addressing the full spectroscopy of low-lying states.

The valence-space in-medium similarity renormalization group (VS-IMSRG) [44, 45, 46, 47, 48] were performed to produce *ab initio* fp-shell valence-space Hamiltonians and consistently evolved $E2$ operators [49], based on NN+3N forces, 1.8/2.0(EM) [23, 24] and ΔNNLO$_{\rm GO}$ [25], derived from chiral EFT. For $E2$ observables, the major source of theory uncertainties in this case is the missing higher-order collective excitations [50, 51]. Already in its leading-order or single-particle form, the $E2$ operator probes the collective quadrupole deformation of the nuclear states as well as the long-range behaviour of the wave functions. This leads to a significantly slower many-body convergence compared to, e.g., energies or radii, when calculations are performed within a spherical basis. Therefore, many-body truncations are the dominant limitation in *ab initio* VS-IMSRG calculations of $E2$ observables. Another source of uncertainty can in principle be correlated with the calculated charge radii of these nuclei. The $E2$ operator is proportional to r^2 (r being the point proton radius), and any

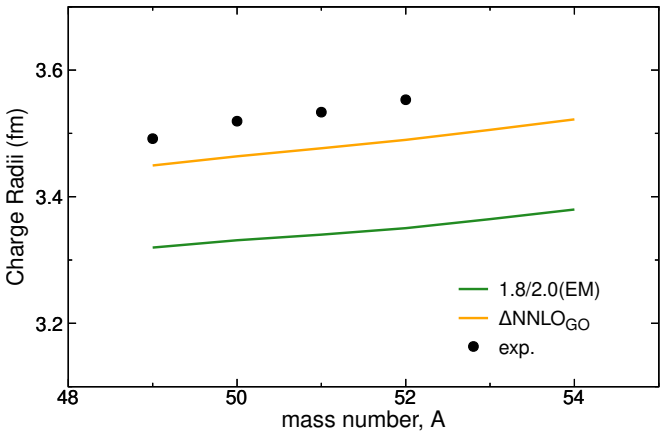


Figure 6: Charge radii in neutron-rich calcium isotopes as a function of mass number. The experimental results [42, 52] are compared with *ab initio* VS-IMSRG predictions utilizing the 1.8/2.0(EM) and ΔNNLO$_{\rm GO}$ interactions.

underprediction in the charge radii could be expected to drive the suppression of $B(E2)$ values. Figure 6 shows the experimental charge radii in neutron-rich Ca isotopes and how they compare with the VS-IMSRG calculations. In particular, we note that those using the ΔNNLO$_{\rm GO}$ interaction are reproducing relatively well the charge radii, and therefore we expect this should not be the major contributor to the underestimation of the $B(E2)$ values.

For the odd-mass cases the agreement of the VS-IMSRG calculations with experiment is generally good, as was similarly seen in ^{21}O [34] and ^{49}Ca [21]. In contrast to shell-model calculations where the $B(E2)$ strength depends on the effective charges, the latter are not relevant to the VS-IMSRG calculations, since the effective operators are calculated consistently, and therefore effective charges are not needed. It is interesting to see that VS-IMSRG (which generally underestimates more collective transitions in even-even isotopes) are closer to the UFP-CA calculations with microscopically-treated effective charges.

The investigation of associated shell model effective charges – and how they arise from many-body mechanisms – is being approached with self-consistent Greens function (SCGF) theory [53]. In this framework, the knowledge of electromagnetic transition strength for neutron-rich calcium isotopes is pivotal to test and improve the SCGF calculations.

5. Conclusion

In summary, the first high-resolution in-beam γ-ray spectroscopy of ^{53}Ca was performed at the RIBF using the HiCARI array. The lifetime of the first excited $5/2^-$ state was determined for the first time through a Doppler line-shape analysis. The resulting $B(E2)$ value is well reproduced by shell-model calculations using the standard neutron effective charge $e_n = 0.5$; however, calculations employing microscopically-treated effective charges and modern *ab initio* approaches substantially underestimate the observed strength. The present result adds to the electromagnetic transition data in the neutron-

rich Ca isotopes, which provide a stringent benchmark for theoretical descriptions of electromagnetic transitions in neutron-rich nuclei. Further experimental investigations, such as systematic measurements of transition probabilities in neutron-rich calcium isotopes via Coulomb excitation will provide a more comprehensive picture of shell evolution in this region.

Acknowledgements

We thank Augusto O. Macchiavelli for insightful discussions. This work was carried out at the RIBF operated by RIKEN Nishina Center and Center for Nuclear Study in the University of Tokyo and we thank the staff for providing stable beams with high intensities to the experiment. We acknowledge the Miniball Collaboration for the loan of the Miniball detectors and the supporting frame. The Research Center for Nuclear Physics in Japan, the Institute of Modern Physics in China, the Lawrence Berkeley National Laboratory, and the Argonne National Laboratory in the USA are acknowledged for the loan of detectors and data acquisition electronics. The HiCARI campaign was supported by the JSPS KAKENHI of Japan under Grants No. Kiban-A JP19H00670 and No. JP19H01914. This work was supported by the Royal Society and the UK STFC under grant numbers ST/P003885/1, ST/V001035/1, and ST/Y000285/1. B. A. B. acknowledges support from NSF Grant No. PHY-2110365. J. D. H. acknowledges support from NSERC under grant SAPIN-2024-0003, and the Arthur B. McDonald Canadian Astroparticle Physics Research Institute. T. M. acknowledges support from JST ERATO Grant No. JPMJER2304, Japan and KAKENHI (25K07294, 25K00995, 25K07330, 26H01394). The VS-IMSRG calculations were performed using the `imsrg++` [54] code. Computations were performed with an allocation of computing resources on Cedar and Fir at WestGrid and the Digital Research Alliance of Canada. B. M. acknowledges support from Institute for Basic Science (Grant Nos. IBS-R031-Y1 and IBS-R031-D1) and National Research Foundation (Grant No. 2019R1A6A3A03031564) of the Republic of Korea. This work is partially supported by JSPS KAKENHI (Grant Nos. 19H00679, 19H01914 and 24H00239)). K. W. acknowledges support from the European Research Council (ERC) under the European Unions Horizon 2020 research and innovation programme (grant agreement No 101001561) and the Deutsche Forschungsgemeinschaft (DFG, German Research Foundation) under Contract No. SFB 1245 (Project ID No. 79384907). H. L. C., P. F. and C. C. acknowledge support from U.S. Department of Energy, Office of Science, Office of Nuclear Physics, under Contract No. DE-AC02-05CH11231 (LBNL).

References

[1] A. Gade, et al., Cross-shell excitation in two-proton knockout: Structure of ^{52}Ca, Phys. Rev. C 74 (2006) 021302. doi:10.1103/PhysRevC.74.021302.
URL https://link.aps.org/doi/10.1103/PhysRevC.74.021302

[2] D. Steppenbeck, et al., Evidence for a new nuclear 'magic number' from the level structure of ^{54}Ca, Nature 502 (7470) (2013) 207–210.
URL https://www.nature.com/articles/nature12522

[3] A. Magilligan, B. A. Brown, S. R. Stroberg, Data-driven configuration-interaction hamiltonian extrapolation to ^{60}Ca, Phys. Rev. C 104 (2021) L051302. doi:10.1103/PhysRevC.104.L051302.
URL https://link.aps.org/doi/10.1103/PhysRevC.104.L051302

[4] S. Chen, et al., Level structures of 56,58Ca cast doubt on a doubly magic 60Ca, Physics Letters B 843 (2023) 138025. doi:https://doi.org/10.1016/j.physletb.2023.138025.
URL https://www.sciencedirect.com/science/article/pii/S0370269323003593

[5] T. Koiwai, et al., A first glimpse at the shell structure beyond 54Ca: Spectroscopy of 55K, 55Ca, and 57Ca, Phys. Lett. B 827 (2022) 136953. doi:https://doi.org/10.1016/j.physletb.2022.136953.
URL https://www.sciencedirect.com/science/article/pii/S0370269322000879

[6] M. Cortés, et al., Shell evolution of $N = 40$ isotones towards ^{60}Ca: First spectroscopy of ^{62}Ti, Phys. Lett. B 800 (2020) 135071. doi:https://doi.org/10.1016/j.physletb.2019.135071.
URL http://www.sciencedirect.com/science/article/pii/S0370269319307932

[7] F. Nowacki, A. Obertelli, A. Poves, The neutron-rich edge of the nuclear landscape: Experiment and theory., Progress in Particle and Nuclear Physics 120 (2021) 103866. doi:https://doi.org/10.1016/j.ppnp.2021.103866.
URL https://www.sciencedirect.com/science/article/pii/S014664102100020X

[8] T. Kubo, et al., BigRIPS separator and ZeroDegree spectrometer at RIKEN RI Beam Factory, Prog. Theor. Exp. Phys. 2012 (1) (2012).
URL http://ptep.oxfordjournals.org/content/2012/1/03C003.abstract

[9] N. Fukuda, et al., Identification and separation of radioactive isotope beams by the BigRIPS separator at the RIKEN RI Beam Factory , Nucl. Instrum. Methods Phys. Res., Sect. B 317, Part B (2013) 323 – 332. doi:http://dx.doi.org/10.1016/j.nimb.2013.08.048.
URL http://www.sciencedirect.com/science/article/pii/S0168583X13009890

[10] K. Wimmer, et al., Hicari: High-resolution cluster array at ribf, RIKEN Accel. Prog. Rep. 54 (2021) S27.
URL https://www.nishina.riken.jp/researcher/APR/APR054/pdf/S27.pdf

[11] N. Warr, J. Van de Walle, M. Albers, F. Ames, B. Bastin, C. Bauer, V. Bildstein, A. Blazhev, S. Bönig, N. Bree, et al., The miniball spectrometer, Eur. Phys. J. A 49 (3) (2013) 40.
URL https://link.springer.com/article/10.1140/epja/i2013-13040-9

[12] W. Hua, N. Zhang, M. Liu, Y. Zheng, Y. Fang, X. Zhou, Y. Zhang, X. Lei, Y. Guo, Brief introduction to the γ-detector array at institute of modern physics in lanzhou, in: Nuclear Structure in China 2012, World Scientific, 2013, pp. 98–100.
URL https://doi.org/10.1142/9789814447485_0016

[13] D. Weisshaar, D. Bazin, P. Bender, C. Campbell, F. Recchia, V. Bader, T. Baugher, J. Belarge, M. Carpenter, H. Crawford, M. Cromaz, B. Elman, P. Fallon, A. Forney, A. Gade, J. Harker, N. Kobayashi, C. Langer, T. Lauritsen, I. Lee, A. Lemasson, B. Longfellow, E. Lunderberg, A. Macchiavelli, K. Miki, S. Momiyama, S. Noji, D. Radford, M. Scott, J. Sethi, S. Stroberg, C. Sullivan, R. Titus, A. Wiens, S. Williams, K. Wimmer, S. Zhu, The performance of the -ray tracking array gretina for -ray spectroscopy with fast beams of rare isotopes, Nucl. Instrum. Methods A 847 (2017) 187–198. doi:https://doi.org/10.1016/j.nima.2016.12.001.
URL https://www.sciencedirect.com/science/article/pii/S0168900216312402

[14] J. Acosta, A. Jungclaus, M. Armstrong, M. Górska, T. Parry, Z. Podolyák, P. Doornenbal, K. Wimmer, A. Gargano, N. Aoi, H. Baba, F. Browne, C. Campbell, H. Crawford, H. de Witte, F. Flavigny, C. Fransen, H. Hess, E. Ideguchi, S. Iwazaki, J. Kim, A. Kohda, T. Koiwai, B. Mauss, R. Mizuno, B. Moon, M. Niikura, R. Orlandi, L. Plagnol, P. Reiter, H. Sakurai, D. Suzuki, R. Taniuchi, S. Thiel, Y. Yamamoto, Excited-state lifetimes in ^{131}In, ^{131}Sn, and ^{136}Te measured with the hicari γ-ray spectrometer at ribf at riken, Phys. Rev. C 111 (2025) 064316. doi:10.1103/mysq-byyv.
URL https://link.aps.org/doi/10.1103/mysq-byyv

[15] S. Paschalis, I. Lee, A. Macchiavelli, C. Campbell, M. Cromaz, S. Gros, J. Pavan, J. Qian, R. Clark, H. Crawford, D. Doering, P. Fallon, C. Lionberger, T. Loew, M. Petri, T. Stezelberger, S. Zimmermann, D. Radford, K. Lagergren, D. Weisshaar, R. Winkler, T. Glasmacher, J. Anderson, C. Beausang, The performance of the gamma-ray energy tracking in-beam nuclear array gretina, Nucl. Instrum. Methods Phys. Res., Sect. A 709 (2013) 44–55. doi:https://doi.org/10.1016/j.nima.2013.01.009.
URL https://www.sciencedirect.com/science/article/pii/S0168900213000508

[16] S. Agostinelli, et al., Geant4–a simulation toolkit , Nucl. Instrum. Methods Phys. Res., Sect. A 506 (3) (2003) 250 – 303. doi:http://dx.doi.org/10.1016/S0168-9002(03)01368-8.
URL http://www.sciencedirect.com/science/article/pii/S0168900203013688

[17] L. Riley, D. Weisshaar, H. Crawford, M. Agiorgousis, C. Campbell, M. Cromaz, P. Fallon, A. Gade, S. Gregory, E. Haldeman, L. Jarvis, E. Lawson-John, B. Roberts, B. Sadler, C. Stine, Ucgretina geant4 simulation of the gretina gamma-ray energy tracking array, Nucl. Instrum. Methods Phys. Res., Sect. A 1003 (2021) 165305. doi:https://doi.org/10.1016/j.nima.2021.165305.
URL https://www.sciencedirect.com/science/article/pii/S0168900221002898

[18] National Nuclear Data Center, Evaluated nuclear structure data file (ensdf), https://www.nndc.bnl.gov/ensdf/, accessed: 2025.

[19] S. Chen, et al., Quasifree Neutron Knockout from ^{54}Ca Corroborates Arising $N = 34$ Neutron Magic Number, Phys. Rev. Lett. 123 (2019) 142501. doi:10.1103/PhysRevLett.123.142501.
URL https://link.aps.org/doi/10.1103/PhysRevLett.123.142501

[20] F. Perrot, F. Maréchal, C. Jollet, P. Dessagne, J.-C. Angélique, G. Ban, P. Baumann, F. Benrachi, U. Bergmann, C. Borcea, A. Buţă, J. Cederkall, S. Courtin, J.-M. Daugas, L. M. Fraile, S. Grévy, A. Jokinen, F. R. Lecolley, E. Liénard, G. L. Scornet, V. Méot, C. Miehé, F. Negoiţă, N. A. Orr, S. Pietri, E. Poirier, M. Ramdhane, O. Roig, I. Stefan, W. Wang, β-decay studies of neutron-rich k isotopes, Phys. Rev. C 74 (2006) 014313. doi:10.1103/PhysRevC.74.014313.
URL https://link.aps.org/doi/10.1103/PhysRevC.74.014313

[21] D. Montanari, et al., Probing the nature of particlecore couplings in 49Ca with γ spectroscopy and heavy-ion transfer reactions, Phys. Lett. B 697 (4) (2011) 288–293. doi:https://doi.org/10.1016/j.physletb.2011.01.046.
URL https://www.sciencedirect.com/science/article/pii/S0370269311000839

[22] J. J. Valiente-Dobón, et al., Lifetime Measurements of the Neutron-Rich $N = 30$ Isotones ^{50}Ca and ^{51}Sc: Orbital Dependence of Effective Charges in the fp Shell, Phys. Rev. Lett. 102 (2009) 242502. doi:10.1103/PhysRevLett.102.242502.
URL https://link.aps.org/doi/10.1103/PhysRevLett.102.242502

[23] K. Hebeler, S. K. Bogner, R. J. Furnstahl, A. Nogga, A. Schwenk, Improved nuclear matter calculations from chiral low-momentum interactions, Phys. Rev. C 83 (2011) 031301(R). doi:10.1103/PhysRevC.83.031301.

URL https://link.aps.org/doi/10.1103/PhysRevC.83.031301

[24] J. Simonis, S. R. Stroberg, K. Hebeler, J. D. Holt, A. Schwenk, Saturation with chiral interactions and consequences for finite nuclei, Phys. Rev. C 96 (2017) 014303. doi:10.1103/PhysRevC.96.014303.
URL https://link.aps.org/doi/10.1103/PhysRevC.96.014303

[25] W. G. Jiang, A. Ekström, C. Forssén, G. Hagen, G. R. Jansen, T. Papenbrock, Accurate bulk properties of nuclei from $A = 2$ to ∞ from potentials with Δ isobars, Phys. Rev. C 102 (2020) 054301. doi:10.1103/PhysRevC.102.054301.
URL https://link.aps.org/doi/10.1103/PhysRevC.102.054301

[26] A. Bohr, B. Mottelson, Nuclear Structure, vol 2, Benjamin, 1975.

[27] M. Petri, P. Fallon, A. O. Macchiavelli, S. Paschalis, K. Starosta, T. Baugher, D. Bazin, L. Cartegni, R. M. Clark, H. L. Crawford, M. Cromaz, A. Dewald, A. Gade, G. F. Grinyer, S. Gros, M. Hackstein, H. B. Jeppesen, I. Y. Lee, S. McDaniel, D. Miller, M. M. Rajabali, A. Ratkiewicz, W. Rother, P. Voss, K. A. Walsh, D. Weisshaar, M. Wiedeking, B. A. Brown, Lifetime measurement of the 2_1^+ state in ^{20}C, Phys. Rev. Lett. 107 (2011) 102501. doi:10.1103/PhysRevLett.107.102501.
URL https://link.aps.org/doi/10.1103/PhysRevLett.107.102501

[28] H. Sagawa, X. R. Zhou, X. Z. Zhang, T. Suzuki, Deformations and electromagnetic moments in carbon and neon isotopes, Phys. Rev. C 70 (2004) 054316. doi:10.1103/PhysRevC.70.054316.
URL https://link.aps.org/doi/10.1103/PhysRevC.70.054316

[29] B. Longfellow, D. Weisshaar, A. Gade, B. A. Brown, D. Bazin, K. W. Brown, B. Elman, J. Pereira, D. Rhodes, M. Spieker, Quadrupole collectivity in the neutron-rich sulfur isotopes ^{38,40,42,44}S, Phys. Rev. C 103 (2021) 054309. doi:10.1103/PhysRevC.103.054309.
URL https://link.aps.org/doi/10.1103/PhysRevC.103.054309

[30] A. Poves, J. Sánchez-Solano, E. Caurier, F. Nowacki, Shell model study of the isobaric chains $A = 50$, $A = 51$ and $A = 52$, Nucl. Phys. A 694 (1) (2001) 157 – 198. doi:https://doi.org/10.1016/S0375-9474(01)00967-8.
URL http://www.sciencedirect.com/science/article/pii/S0375947401009678

[31] M. Honma, T. Otsuka, B. A. Brown, T. Mizusaki, Shell-model description of neutron-rich pf-shell nuclei with a new effective interaction GXPF1, Eur. Phys. J. A 25 (1) (2005) 499–502. doi:10.1140/epjad/i2005-06-032-2.
URL https://doi.org/10.1140/epjad/i2005-06-032-2

[32] T. H. Ogunbeku, et al., Universal effective charges in the *sd* and *fp* shells, Phys. Rev. Lett. 135 (2025) 072501. doi:10.1103/75ry-71sj.
URL https://link.aps.org/doi/10.1103/75ry-71sj

[33] B. A. Brown, K. Minamisono, β^2 corrections to spherical energy-density functional calculations for root-mean-square charge radii, Phys. Rev. C 106 (2022) L011304. doi:10.1103/PhysRevC.106.L011304.
URL https://link.aps.org/doi/10.1103/PhysRevC.106.L011304

[34] S. Heil, M. Petri, K. Vobig, D. Bazin, J. Belarge, P. Bender, B. Brown, R. Elder, B. Elman, A. Gade, T. Haylett, J. Holt, T. Hüther, A. Hufnagel, H. Iwasaki, N. Kobayashi, C. Loelius, B. Longfellow, E. Lunderberg, M. Mathy, J. Menéndez, S. Paschalis, R. Roth, A. Schwenk, J. Simonis, I. Syndikus, D. Weisshaar, K. Whitmore, Electromagnetic properties of 21O for benchmarking nuclear Hamiltonians, Phys. Lett. B 809 (2020) 135678. doi:https://doi.org/10.1016/j.physletb.2020.135678.
URL https://www.sciencedirect.com/science/article/pii/S0370269320304810

[35] B. A. Brown, W. A. Richter, New "usd" hamiltonians for the *sd* shell, Phys. Rev. C 74 (2006) 034315. doi:10.1103/PhysRevC.74.034315.
URL https://link.aps.org/doi/10.1103/PhysRevC.74.034315

[36] W. A. Richter, S. Mkhize, B. A. Brown, *sd*-shell observables for the USDA and USDB Hamiltonians, Phys. Rev. C 78 (2008) 064302. doi:10.1103/PhysRevC.78.064302.
URL https://link.aps.org/doi/10.1103/PhysRevC.78.064302

[37] B. Brown, A. Arima, J. McGrory, E2 core-polarization charge for nuclei near 16O and 40Ca, Nuclear Physics A 277 (1) (1977) 77–108. doi:https://doi.org/10.1016/0375-9474(77)90263-9.
URL https://www.sciencedirect.com/science/article/pii/0375947477902639

[38] G. Hagen, M. Hjorth-Jensen, G. R. Jansen, R. Machleidt, T. Papenbrock, Evolution of Shell Structure in Neutron-Rich Calcium Isotopes, Phys. Rev. Lett. 109 (2012) 032502. doi:10.1103/PhysRevLett.109.032502.
URL https://link.aps.org/doi/10.1103/PhysRevLett.109.032502

[39] J. D. Holt, J. Menendez, A. Schwenk, The role of three-nucleon forces and many-body processes in nuclear pairing, J. Phys. G 40 (2013) 075105. doi:10.1088/0954-3899/40/7/075105.

[40] J. D. Holt, J. Menéndez, J. Simonis, A. Schwenk, Three-nucleon forces and spectroscopy of neutron-rich calcium isotopes, Phys. Rev. C 90 (2014) 024312. doi:10.1103/PhysRevC.90.024312.
URL https://link.aps.org/doi/10.1103/PhysRevC.90.024312

[41] F. Wienholtz, et al., Masses of exotic calcium isotopes pin down nuclear forces, Nature 498 (7454) (2013) 346–349.
URL https://www.nature.com/articles/nature12226

[42] R. Garcia Ruiz, et al., Unexpectedly large charge radii of neutron-rich calcium isotopes, Nature Physics (2 2016). doi:10.1038/nphys3645.

[43] B. S. Hu, A. Ekström, C. Forssén, G. Hagen, W. G. Jiang, T. Miyagi, T. Papenbrock, The neutron dripline in calcium isotopes from a chiral interaction (2025). arXiv:2512.11723.
URL https://arxiv.org/abs/2512.11723

[44] K. Tsukiyama, S. K. Bogner, A. Schwenk, In-Medium Similarity Renormalization Group For Nuclei, Phys. Rev. Lett. 106 (2011) 222502. doi:10.1103/PhysRevLett.106.222502.
URL http://link.aps.org/doi/10.1103/PhysRevLett.106.222502

[45] H. Hergert, S. K. Bogner, T. D. Morris, A. Schwenk, K. Tsukiyama, The in-medium similarity renormalization group: A novel ab initio method for nuclei, Phys. Rep. 621 (2016) 165 – 222. doi:10.1016/j.physrep.2015.12.007.
URL http://www.sciencedirect.com/science/article/pii/S0370157315005414

[46] S. R. Stroberg, A. Calci, H. Hergert, J. D. Holt, S. K. Bogner, R. Roth, A. Schwenk, Nucleus-dependent valence-space approach to nuclear structure, Phys. Rev. Lett. 118 (2017) 032502. doi:10.1103/PhysRevLett.118.032502.
URL https://link.aps.org/doi/10.1103/PhysRevLett.118.032502

[47] S. R. Stroberg, S. K. Bogner, H. Hergert, J. D. Holt, Nonempirical Interactions for the Nuclear Shell Model: An Update, Ann. Rev. Nucl. Part. Sci. 69 (2019) 307–362. arXiv:1902.06154, doi:10.1146/annurev-nucl-101917-021120.

[48] B. Hu, W. Jiang, T. Miyagi, Z. Sun, A. Ekström, C. Forssén, G. Hagen, J. D. Holt, T. Papenbrock, S. R. Stroberg, I. Vernon, Ab initio predictions link the neutron skin of ^{208}Pb to nuclear forces, Nature Physics 18 (10) (2022) 1196–1200. doi:10.1038/s41567-022-01715-8.
URL https://doi.org/10.1038/s41567-022-01715-8

[49] N. M. Parzuchowski, S. R. Stroberg, P. Navrátil, H. Hergert, S. K. Bogner, Ab initio electromagnetic observables with the in-medium similarity renormalization group, Phys. Rev. C 96 (3) (2017) 034324. arXiv:1705.05511, doi:10.1103/PhysRevC.96.034324.

[50] J. Henderson, et al., Testing microscopically derived descriptions of nuclear collectivity: Coulomb excitation of ^{22}Mg, Phys. Lett. B 782 (2018) 468–473. arXiv:1709.03948, doi:10.1016/j.physletb.2018.05.064.

[51] S. R. Stroberg, J. Henderson, G. Hackman, P. Ruotsalainen, G. Hagen, J. D. Holt, Systematics of E2 strength in the sd shell with the valence-space in-medium similarity renormalization group, Phys. Rev. C 105 (3) (2022) 034333. doi:10.1103/PhysRevC.105.034333.

[52] G. Co', M. Anguiano, A. M. Lallena, Charge radii of ca isotopes and correlations, Phys. Rev. C 105 (2022) 034320. doi:10.1103/PhysRevC.105.034320.
URL https://link.aps.org/doi/10.1103/PhysRevC.105.034320

[53] F. Raimondi, C. Barbieri, Core-polarization effects and effective charges in O and Ni isotopes from chiral interactions, Phys. Rev. C 100 (2019) 024317. doi:10.1103/PhysRevC.100.024317.
URL https://link.aps.org/doi/10.1103/PhysRevC.100.024317

[54] S. R. Stroberg, imsrg++, https://github.com/ragnarstroberg/imsrg (2026).
URL https://github.com/ragnarstroberg/imsrg